water

MDPI

Article

Low Altitude Unmanned Aerial Vehicles (UAVs) and Satellite Remote Sensing Are Used to Calculated River Discharge Attenuation Coefficients of Ungauged Catchments in Arid Desert

Shengtian Yang [1,2,3], Juan Wang [3,4], Pengfei Wang [1], Tongliang Gong [5] and Huiping Liu [3,4,*]

1 College of Water Sciences, Beijing Normal University, Beijing 100875, China; yangshengtian@bnu.edu.cn (S.Y.); wangpengfei199403@163.com (P.W.)
2 Beijing Key Laboratory of Urban Hydrological Cycle and Sponge City Technology, Beijing 100875, China
3 Beijing Key Laboratory of Environmental Remote Sensing and Digital Cities, Beijing Normal University, Beijing 100875, China; wangjuan6231@163.com
4 School of Geography, Faculty of Geographical Science, Beijing Normal University, Beijing 100875, China
5 Bureau of Hydrological and Water Resources Survey of Tibet Autonomous Region, Lhasa 850000, China; 13908902602@139.com
* Correspondence: hpliu@bnu.edu.cn

Received: 25 October 2019; Accepted: 10 December 2019; Published: 13 December 2019

Abstract: The arid desert ecosystem is very fragile, and the change of its river discharge has a direct impact on irrigation and natural environment. River discharge attenuation coefficients is a key index to reveal the stability of desert river ecosystem. However, due to the harsh conditions in desert areas, it is difficult to establish a hydrological station to obtain data and calculate the attenuation coefficients, so it is urgent to develop new methods to master the attenuation coefficients of rivers. In this study, Taklamakan desert river was selected as the research area, and the river discharge of the desert river were estimated by combining low-altitude UAV and satellite remote sensing technology, so as to calculate the attenuation status of the river in its natural state. Combined with satellite remote sensing, the surface runoff in the desert reaches of the Hotan River from 1993 to 2017 were estimated. The results showed that the base of runoff attenuation in the lower reaches of the Hotan River is 40%. Coupled UAV and satellite remote sensing technology can provide technical support for the study of surface runoff in desert rivers within ungauged basins. Using UAV and satellite remote sensing can monitor surface runoff effectively providing important reference for river discharge monitoring in ungauged catchments.

Keywords: desert river; attenuation coefficients; ungauged basin; unmanned aerial vehicle (UAV); satellite remote sensing

1. Introduction

The flow of arid desert river affects the stability of regional ecosystem and plays a vital role in maintaining the biodiversity and ecosystem integrity of the river [1–3]. Therefore, the availability of river discharges in ungauged catchments of arid desert is of great concern [4,5]. In recent years, the study of desert rivers has attracted the attention of many scholars [4,6], but in the past, there were more attention to the quaternary geology, paleoenvironment and fluvial geomorphologic evolution [7,8], and there is a lack of quantitative expression of river discharge [6]. There is a great obstacle to the study of surface runoff in ungauged catchments of arid desert, and it is difficult to meet the demand of hydrological monitoring data for current global change research.

The attenuation coefficients of river discharge is the key index for maintaining fluvial ecosystems and arises through evaporation and infiltration during transport, which is usually calculated from the flow rate during the dry season [9,10]. The process of driving river attenuation depends on a series of physicochemical and biological parameters such as river velocity, temperature, vertical hydrological exchange of surface runoff and groundwater [11,12]. In the past 30 years, some relatively mature computational methods have been developed [13–16], which can be mainly divided into hydrological methods, hydraulic methods, habitat simulation methods and holistic analysis methods. These methods require a lot of information and require a long time of investigation, which tends to be carried out in areas with abundant hydrological data. However, large portions of total River Basins across the globe are either poorly gauged or completely ungauged [17–19], and hydrological observation networks are continuously deteriorating [20]. Therefore, there is a lack of research on surface runoff in ungauged catchments of arid desert [21–23], and the study on river attenuation is basically blank, resulting in high variability of attenuation rate in rivers, which complicates the prediction of environmental flows [24,25].

Calculating the streamflow in ungauged catchments is surrounded by uncertainty, and is thus a challenging, yet vital task for water management. New and easily accessible satellite data have been increasingly steadily in recent years. Many studies have been conducted using satellite data to estimate river discharge [26–28]. Traditional methods for estimating river discharge mainly adopt the following methods: (1) Numerical simulation Equation [29,30], where most of the parameters are obtained through laboratory experiments, and some parameters are difficult to be obtained, so only field measurement can be used for inversion analysis. (2) Empirical Equation [31,32], which is derived from Manning-Strickler Equation or Chezy Equation, and then summarized from experimental observation; (3) Based on data statistics or machine learning method [33,34], this method needs a large amount of data to predict by machine learning theory. In general, the application of traditional estimation methods is limited by the large amount of field observation data. At present, satellite data, as a new and easily accessible data source, has been growing steadily in recent years. Many scholars combine satellite data with traditional estimation methods to study the river discharge [27,35,36]. Over the years, the use of satellite remote sensing data for research on runoff has mostly focused on using the measured data to analyze hydrological characteristics, changes in annual runoff, current hydrological conditions, and the availability of water resources [37,38]. Satellite remote sensing data can only monitor large rivers with large volumes of water, and it is difficult to calculate fluvial runoff for small volumes of water, which makes it difficult to verify the distributed hydrological models developed based on remote sensing data. Therefore, new, high-resolution data sources are needed to improve upon the existing methods.

Over the past 5 years, remote sensing based on unmanned aerial vehicles (UAVs) has rapidly expanded in the field of civil use [39]. UAVs is one technology able to fill the gap between spaceborne and ground-based observations, ensuring (1) high spatial resolution; (2) tracking of the water bodies better than any satellite technology; (3) operating an UAV is not limited to specific time, such as satellite sensors that synchronize with the sun; (4) flexibility of the payload. Therefore, the use of UAV to quickly obtain topographic data, combined with field measurement data, makes up for most of the small and medium-sized River Basins that are not suitable for station construction but still need discharge monitoring.

The research has shown that UAV-based image acquisition is suitable for environmental remote sensing and monitoring [40–43]. UAV data has also been widely used in the field of river monitoring, e.g., evaluating the ecological environment flow [44], monitoring river morphology and riparian erosion [45,46], estimating river discharges in ungauged catchments [47], etc. These method have strong practicability for obtaining river sections in poorly gauged area, and can be regarded as a new method for obtaining and analyzing flow information in poorly gauged area [48–50].

In this study, the typical river runoff in the Taklamakan Desert were selected as the research subject. Generally, due to geographical limitations, it is difficult to obtain in-depth data by conventional means, as the width-depth ratio of cross section is large for the wide-shallow rivers in arid scarcity areas, which can reflect the change of discharge in different periods. Therefore, for such unmeasured rivers, low-altitude UAV data was carefully combined with satellite remote sensing data to estimate the river discharge, and to further estimate the attenuation coefficients of the river in its natural state. The objectives of this study were to: (1) acquire the digital surface model (DSM) data of river sections from UAV, with which the shapes of river sections were determined, (2) calculate the river discharge by UAV and satellite remote sensing, and (3) obtain the attenuation coefficients of desert rivers. Finally, the attenuation pattern of surface runoff in desert rivers in this extremely arid climate was revealed, providing insights into the effects of global climate change in this region for hydrological monitoring.

2. Study Area

The Taklamakan Desert, located in the middle latitudes of Eurasia in the Northern Hemisphere, is famous for its extremely dry climate and the second largest mobile desert in the world. It also serves as an indicator of global climate change [3,51]. The Taklamakan Desert exhibits unique patterns in its material energy and water circulation. Its material and energy transport are important influences on the circulation of the atmosphere in Central Asia [52,53]. At present, the ecological environment, fluvial resources, and hydrological characteristics of the Taklamakan Desert have attracted global attention [54,55]. In the Taklamakan Desert, the main aquatic systems are the Hotan, Yerqiang, Weigan, and Aksu river systems, as well as the Bosten lake system. Among them, Hotan River Basin is adjacent to Yerqiang River Basin, as shown in Figure 1. The Hotan River spans from Mount Muztagh Ata at an altitude of 6638 m in the northern Tibetan Plateau to the Tarim Basin, crossing the Taklamakan Desert into the Tarim Basin after ~500 km; it is currently the only river that ranges throughout the renowned desert [56]. The Yerqiang river is located in the west of Taklamakan Desert and has similar geographical environment and climatic conditions with Hotan river.

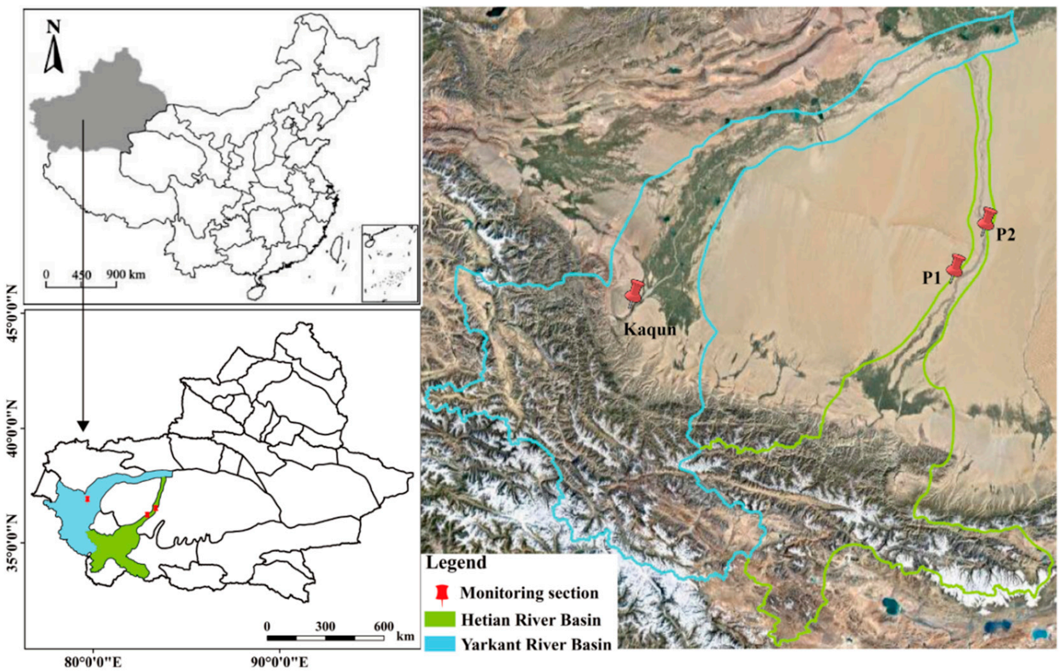

Figure 1. Regional setting of the Yarkant River Basin and Hotan River Basin.

Along the banks of the river are Populus euphratica forests, Tamarix sp., licorice, Alhagi sp., and a few reeds. The variation of desert river discharge is very important to the diversity of coastal ecosystem and the utilization of downstream water resources. However, due to the lack of hydrological observation data along the way, runoff and the patterns thereof remain poorly controlled. Therefore, Yerqiang River Basin and Hotan River Basin are selected as research areas to estimate the river discharge of desert rivers and discuss the attenuation coefficients of desert rivers, so as to provide reference for the utilization of desert rivers.

3. Methodology

3.1. Estimated River Discharge

Flow velocity Equations from local-scale models can be parameterized with specific catchment values. However, flow velocities have to be modelled enough to derive the required parameters from data available for the study region and sophisticated enough to deliver realistic flow velocity values for a large variety of environmental conditions. The Manning Equation was proposed in accordance with 200 experimental data [57], reflecting the relationship between water flow and a river bed, as well as internal factors of a river bed [58,59]. Current research mainly focuses on the hydrologic characteristics of uniform flow and the Manning coefficient, which simplifies non-uniform flow to a uniform flow state [32]. The approximate flow state is considered uniform in a traditional open channel with no vegetation on a large scale. In this case, the Manning Equation can be used to directly quantify the relationship between the Manning coefficient, velocity and water depth. In a few global scale models, the Manning-Strickler Equation has been applied to simulate variable river flow velocities [31,60], which led to enhanced representations of flow velocities [31] and discharge [60]. The Manning-Strickler Equation for calculating river discharge is:

$$Q = \frac{1}{n} A \left(\frac{A}{P}\right)^{\frac{2}{3}} S^{\frac{1}{2}} \tag{1}$$

where n is the field roughness value. A is the area of the cross-section, m^2. and P is the wet perimeter. S is the hydraulic slop. In general, the relationship between river width and discharge varies between different cross sections, which prompts the question of how the relationship between width and flow changes with narrow rivers and wide and shallow rivers in arid data-poor areas. According to the field investigation, the Taklamakan Desert river can be mainly categorized into trapezoidal section (Figure 2).

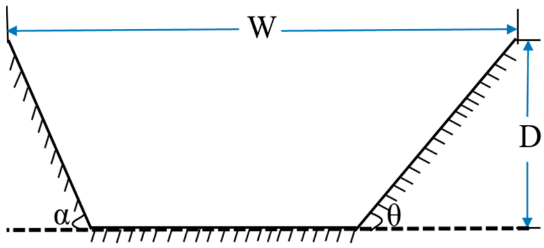

Figure 2. Outline of trapezoidal section (Revised from [61]), where, W is the width of the water surface; D the depth of the water; α and θ are the angles of the river bank.

According to Huang [61], the river discharge of trapezoidal section can be estimated by using altimetry satellite and optical image. However, in a data-poor area, it is difficult to obtain effective water depth data from medium-sized and small, wide and shallow rivers because the depth extraction error is large from a lack of verification points and poor data quality from satellite altimetry. Therefore, satellite altimetry is not suitable for wide and shallow rivers in the arid and data-poor areas in northwestern China. According to Huang [61], the roughness coefficient (n) and slope (S) are considered as constants to avoid using them as dynamic variables. Based on this hypothesis and the characteristics of rivers in arid areas, this study determined coefficient c and water depth index (f) to describe the relationship between water depth and river discharge using the method proposed by Huang [61] combined with energy Equations (2)–(4) [62]. On this basis, the water depth D [61] was replaced by the water depth (d) in Equation (3), i.e., Equation (5). Finally, for different river sections, river parameters were obtained based on low-altitude UAV images, which were then converted into Equations dependent on different satellite source variables as input data to obtain the river discharge estimation method of this study Equation (6).

$$w = aQ^b \tag{2}$$

$$d = cQ^f \tag{3}$$

$$v = kQ^m \tag{4}$$

$$Q = aw(cQ^f)^{\frac{5}{3}} \tag{5}$$

$$Q = \sqrt[3]{\left(\frac{1}{acW}\right)^{5f-3}} \tag{6}$$

where, Q is flow rate, a, c, f is coefficient, and W is river width. According to the field measured flow, the unknown parameter a is optimized. The specific calculation method of parameter can be referred to Huang [61]. Given that discharge is related to river width, cross-section, and water depth, understanding these basic hydraulic variables is a priority for discharge estimation.

3.2. Validating the River Section Shape by UAV

Small consumer UAV has the advantages of being easy to use, low cost, high efficiency and flexible flight [63,64]. At present, research showed that the precision of terrain measurement based on UAV can reach centimeters [65]. In this study, an UAV was employed to acquire high-resolution stereoscopic images, which were used to obtain high-resolution topographic data. The measurement setup consisted of an UAV DJI Phantom 4 Professional including a Cardan suspension and an action-camera FC300X_3.6_4000x3000 edition. Stereoscopic images were processed by the rapid and automatic professional processing software Pix4Dmapper (https://pix4d.com/). Pix4Dmapper not only supports UAV data, but also supports aerial photography, oblique photography, and close-range photogrammetry. In this study, we conducted flight missions using the DJI Phantom 4 Professional UAV. The flight was controlled by the intelligent flight control software Pix4D capture, with a flying hnine of 150 m. The photo overlap is set to be 70% to ensure the subsequent generation of stereoscopic image pairs, and obtain 1054 high-resolution photos of UAV. Generally, image treatment includes data importing, initial processing, three-dimensional triangulation processing, digital orthophoto map (DOM) generation, and DSM generation [66,67]. Preparation of the aerial flights and image processing corresponded to the scheme in Figure 3.

Due to the lack of data in the desert area of Hotan River Basin, the Kaqun hydrologic station of Yerqiang river in similar basins was selected as the experimental area to discuss the applicability of Equation (6) in estimating the river discharge of medium and small wide shallow rivers in the desert area without data. UAV was used to obtain the above-ground terrain information in order to verify the shape of river section. In this research, the measured data of Total Station were used to verify the results, which included 22 ground control points. The verification method used the relative root-mean-square error (RMSE) to evaluate the accuracy of UAV data [68]. Among them, the underwater terrain was difficult to obtain through the UAV, so the underwater terrain of this section was measured manually with a water gauge, as shown in Figure 4.

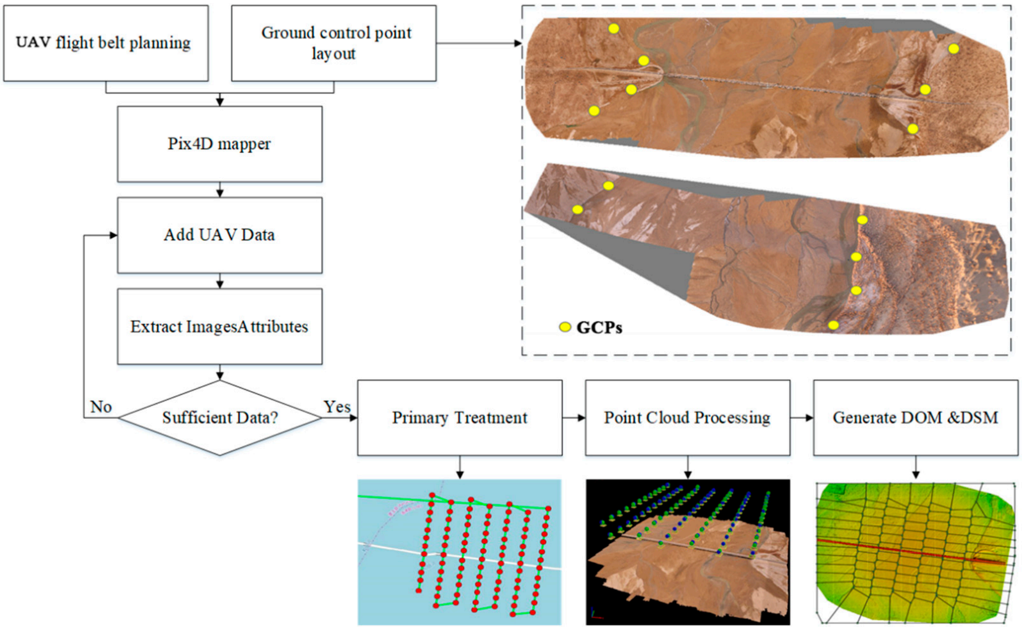

Figure 3. Workflow diagram of the aerial imaging process.

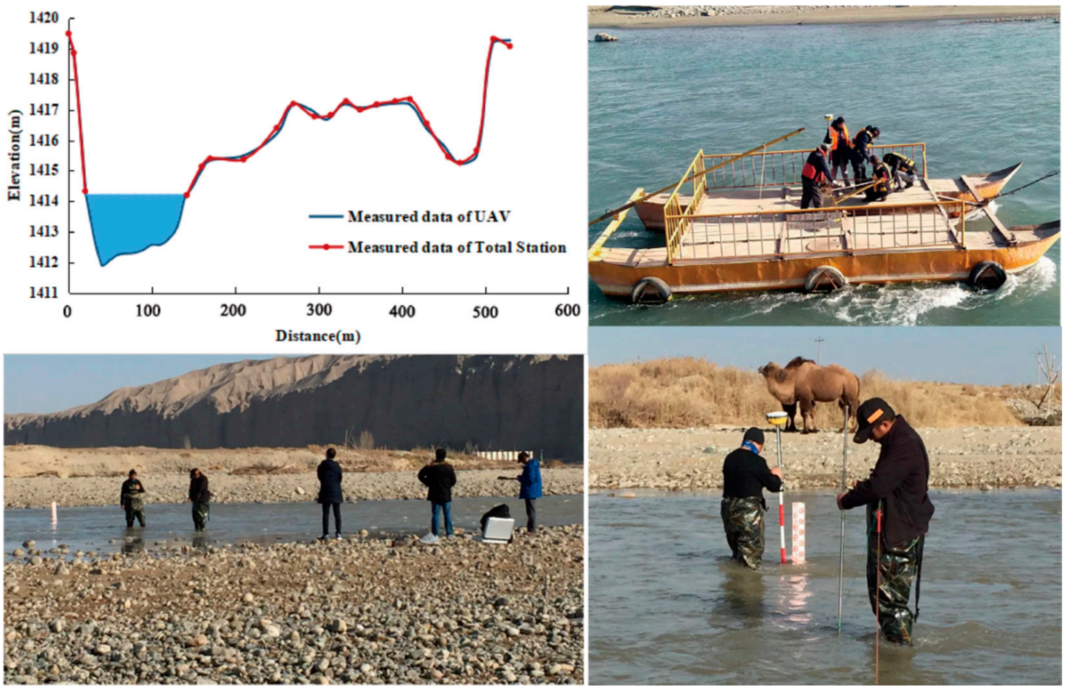

Figure 4. Channel cross-section measured by UAV and the Total Station method.

The elevation of the same point as Ground Control Points (GCPs) were obtained by UAV, and the RMSE was calculated. The results showed that the RMSE error between the UAV data and the topographic measurement data above the river section measured on site was 5.65 cm. It can be seen that the accuracy of river section data obtained by UAV has reached the centimeter level, so we think it is completely feasible to obtain the river section shape by UAV and estimate the river discharge in ungauged catchments area.

3.3. Validating Water Surface Areas by UAV

We used the modified normalized difference water index (MNDWI, see Equation (7)) to extract the width of water surface using Sentnel-2 data (https://scihub.copernicus.eu/). Then the UAV images were used to verify river width (Figure 5) [69].

$$MNDWI = (Green - MIR)/(Green + MIR) \quad (7)$$

where *Green* and *MIR* are the surface reflectance of the green band and middle-infrared band, respectively. Then, we used the maximum between-class variance method [70] to determine the thresholds of binarization for *MNDWI*.

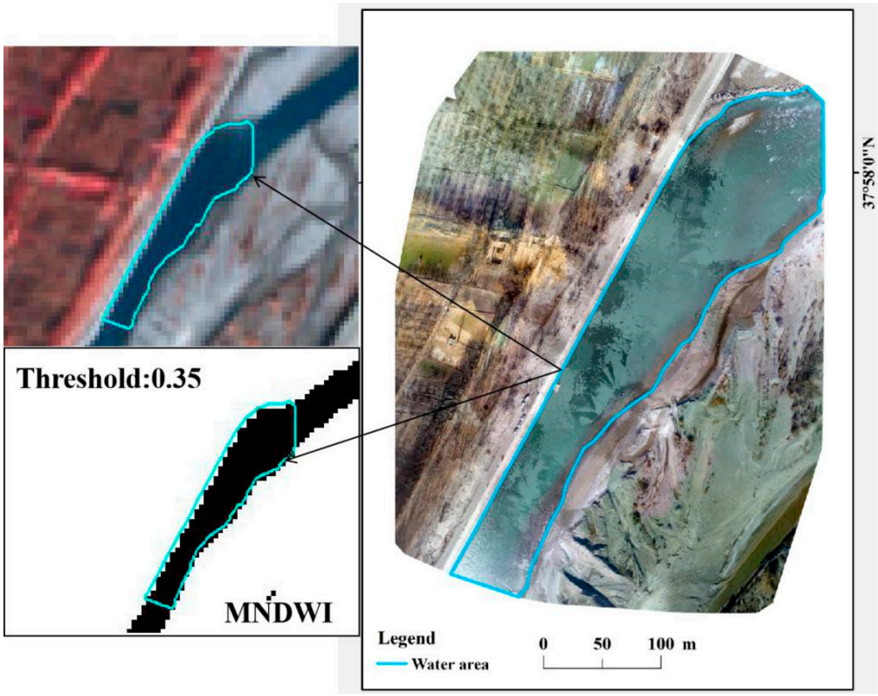

Figure 5. The water boundary extracted by remote sensing image was verified by UAV image at the Kaqun station.

3.4. Performance Metrics

In this study, we selected the root-mean-square error (RMSE) and the Nash-Sutcliffe efficiency coefficient (NSE) [68] to evaluate the discharge estimation performance. The RMSE is used to quantify the deviations of the estimates from the observations. The NSE varies from to 1, and 1 indicates the optimal status where the simulated discharge equals the in situ measurements.

In Kaqun station, the shape of the river sections was obtained by UAV and underwater topography measurement, as shown in Figure 4.

Firstly, the measured average water depth, average velocity and average width data of this hydrologic station from 1998 to 2018 were used to determine the regression coefficient c and water depth index f based on Equations (2)–(4). DSM data were used to obtain the difference between upstream and downstream water levels in river sections. The difference was then divided by the distance between the two points and the ratio, i.e., hydraulic slop, was 0.0019. The coefficient n is empirically derived, which is dependent on many factors, including surface roughness and sinuosity [71]. According to the long-term observation of local hydrographic bureau, the roughness coefficient n is determined to be 0.048. Combined with the field measurement of the side slope of the river section, the obtained data are finally put into Equation (6) as input data. As the Yerqiang river is a seasonal river, we selected hydrographic station data during the summer abundant water period of 2008–2018 (May to September) as the verification data. On this basis, the river discharge was calculated through water surface width of the river section in different periods (Table 1), and verified by comparing with monthly average discharge data of the hydrographic station (Figure 6).

Table 1. Remote-sensing image analysis data for the Yerqiang river reach.

Date	Average Reach Width (m)
10 September 2010	51.5
17 August 2011	158.3
6 August 2013	285.6
6 September 2013	87.1
14 July 2015	127.7
21 August 2015	520.8
18 May 2016	29.2
17 July 2016	383.4
23 May 2017	39.0
25 September 2017	156.8
23 May 2018	155.5
19 June 2018	83.8

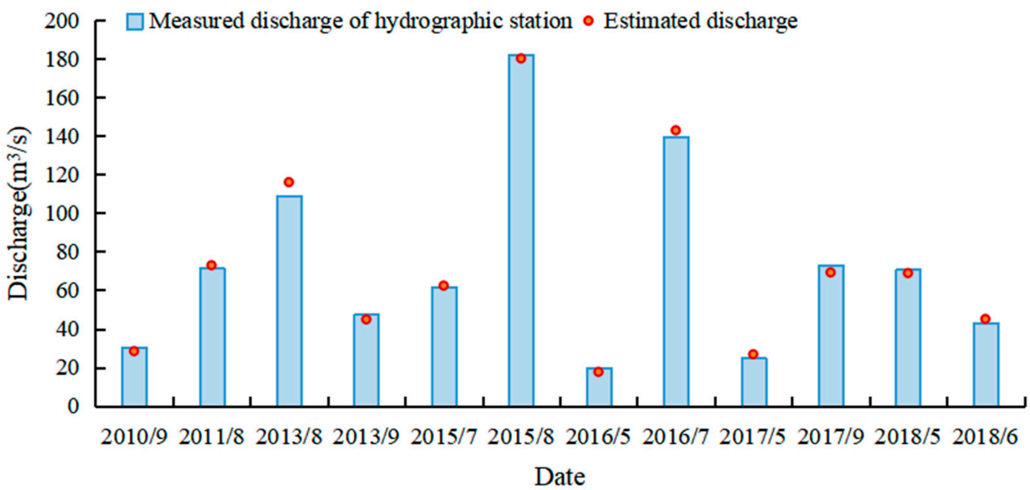

Figure 6. River discharge estimation using Equation (8) in combination with satellite-derived river widths.

Finally, error analysis was conducted on the calculated results, and the RMSE and NSE evaluation results were shown in Table 2. It can be seen that Equation (6) can be used to better estimate the discharge of wide and shallow rivers, indicating that this method is applicable to the estimation of medium and small wide shallow rivers rivers.

Table 2. Equation (6) in river discharge estimation at the Kaqun stations using water widths retrieved from Google.

No. of Samples	RMSE (m^3/s)	NSE
15	2.91	0.996

3.5. Estimated Environmental Flow

On the basis of verifying the applicability of Equation (6), this method is adopted to estimate the river discharge of P1 and P2 monitored sections of the desert reach during dry season in similar basins of Hotan river, where there is a no data area. P1 and P2 sections are 100 km apart, accounting for about

1/5 of the total length of the desert river section. The attenuation coefficient within 100 km of the desert river was discussed to provide a basis for the ecological environment protection of the desert river. Combined with the methods outlined in Sections 3.1 and 3.2, the shapes of the monitored sections were first established, and then the river discharge at P1 and P2 was estimated. Finally, the difference in the river discharge between the two monitored sections was calculated, as shown in Equation (8). The minimum attenuation coefficients of the Hotan River within 100 km was obtained during the dry season.

$$AC = \frac{Q_{p1} - Q_{p2}}{Q_{p1}} \times 100\% \tag{8}$$

where AC is the attenuation coefficients, Q_{P1} is the river discharge at point P1, and Q_{P2} is the river discharge at point P2.

On the bases of the relationships described in Equations (6), combined with high-resolution satellite remote sensing images, the river discharge of Hotan Rivers sections in different periods were estimated, and the changes in the attenuation coefficients during the dry season were then analyzed. In this study, the attenuation coefficients were calculated by using the minimum river discharge during the dry season. The lowest attenuation coefficients within 100 km of the Hotan River under the condition of extreme drought during the dry season was analyzed.

4. Data

4.1. UAV Data

Nine flight missions in Hotan River in the Taklamakan Desert were conducted using the DJI Phantom 4 Professional UAV during the period from 1 December to 2 December of 2017. The flight was controlled by the intelligent flight control software Pix4Dcapture, and the photo overlap was set to 70% to ensure the subsequent generation of stereoscopic image pairs. There were 7 flights in P1 sample area and 2 flights in the P2 sample area, in which the flight height was 160 m and each flight number was 5. A total of 795 photos were obtained from the P1 sample area, and 505 photos were taken from the P2 sample area. The Pix4Dmapper software was then used to extract the modern point cloud and DSM of P1 and P2 (Figure 7). The obtained DOM and DSM data spaces are referred to as WGS1993/UTM zone 48N.

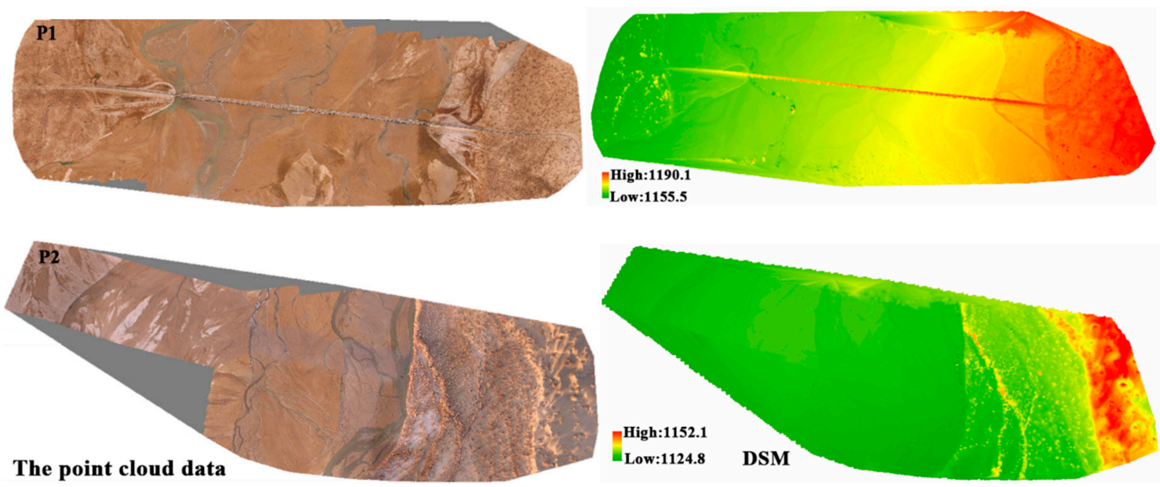

Figure 7. Point cloud data and digital surface model (DSM) map of monitoring stations (**P1**) and (**P2**) in the study area.

4.2. Remote Sensing Data

In this study, Landsat images data were used for detecting changes in water surface area of the Hotan River in the study area. The details are shown in Table 3.

Table 3. Distribution of Hotan River cross sections.

Site	Location	Time	River
P1	38°37′11.72″, 80°57′32.34″	30 November 1993 7 November 1999 20 October 2010	Hotan river
P2	38°11′36.37″, 80°35′55.89″	30 November 1993 7 November 1999 20 October 2010	Hotan river

4.3. Ground-Based Data

At the monitoring stations (P1 and P2), water depth was concurrently measured by using a measuring tape. At the same time, the edge slope (horizontal Angle α, θ) of the river section was measured using a level. In addition to field measured data, monthly average runoff data were collected from the Hotan River from 1964 to 2008. According to the research of Wang [72], monthly average runoff was divided into annual groups. Among them, the upstream river inflow, which was greater than 5 billion m^3, was in the group of abundant water, the upstream river inflow, which ranged between 4 billion m^3 and 5 billion m^3, was in the group of horizontal water, and the upstream river inflow, which was less than 4 billion m^3, was in the group of dry water.

5. Results

5.1. Acquired Features of River Cross Sections Via UAV Imagery

From the high-resolution UAV images, it can be seen that the river runs through the desert, and that the river is winding and branching, as shown in Figure 8. Combined with such images, it can be seen from the monitoring sections P1 and P2 that the river runs through the desert with relatively small fluctuations in surface area, but the river meanders and is more bifurcated. The river, in these sections, has a large amplitude in the desert, and the direction of the local area changes greatly. However, the position of the river bed has changed slightly over the years, and the river bed and the rocks on both banks are composed of silty sand.

Since the Hotan River is a seasonal river, no water flows through it during the dry season, and the river bed is exposed to the surface. The data obtained during this period can then be regarded as a water-free section. However, in the study area, the internal part of the channel is not completely free of water. Therefore, to determine a more accurate shape of the section, water depth measurements were acquired for large sections that had water. Finally, DSM data were combined with the water depth data to determine the river section morphology during the dry season. The shapes of these sections of the river are shown in Figure 9.

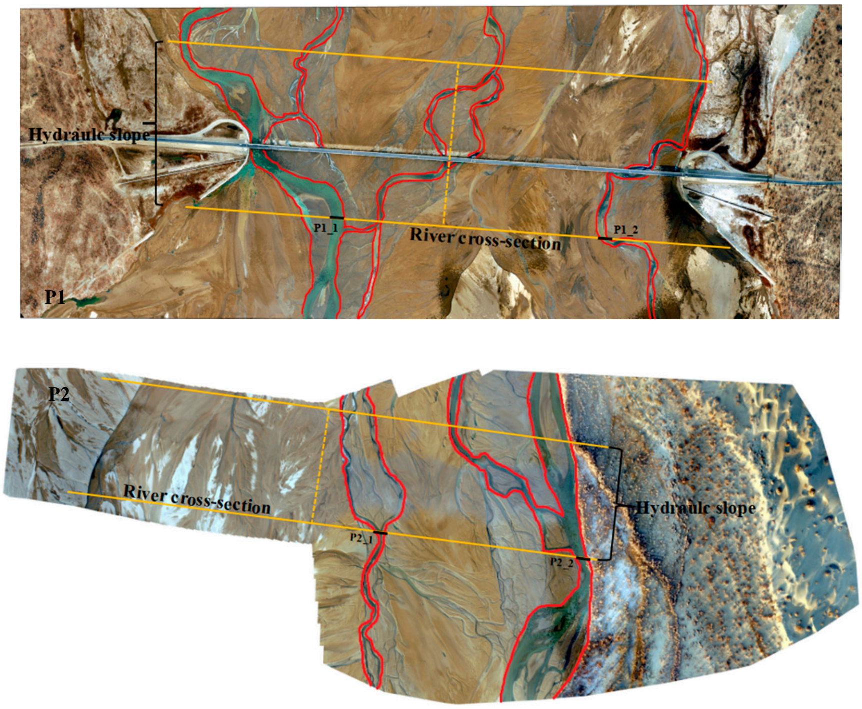

Figure 8. River course cross sections.

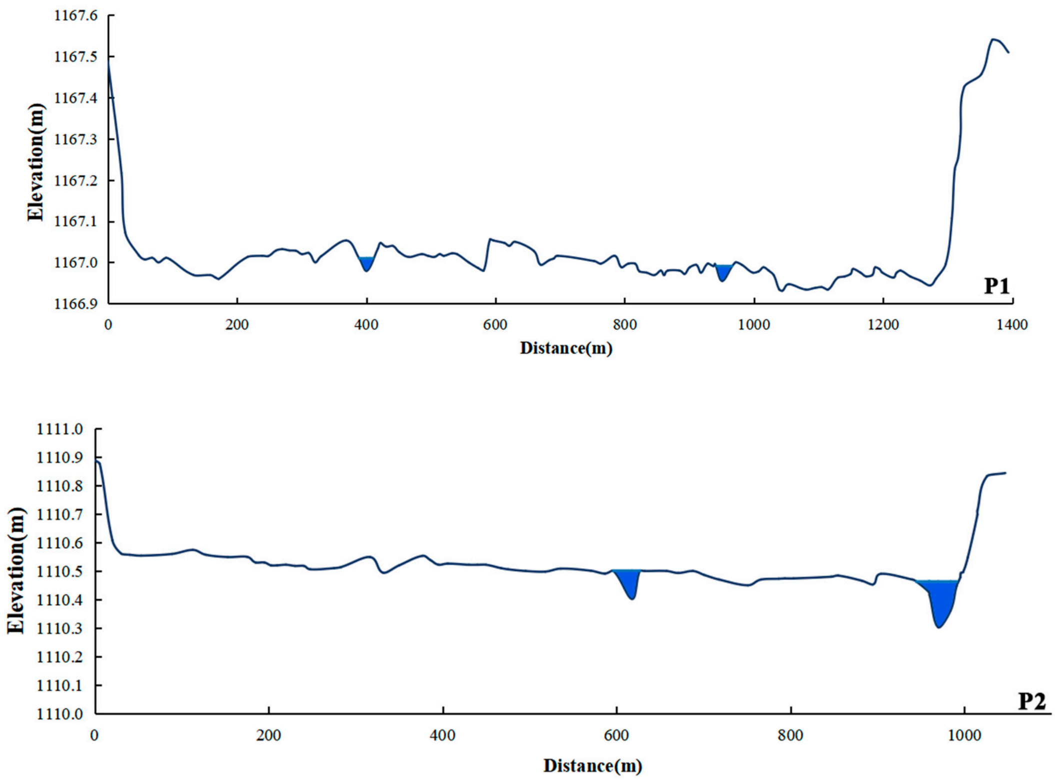

Figure 9. Section from of the desert reaches of the Hotan River.

5.2. Calculated Attenuation Coefficient in the Desert Reaches of the Hotan River

River section DSM data were obtained using high-precision images of a low-altitude UAV. Then, the hydraulic slope of each river section was calculated. Based on Equations (2)–(4), the section data of the upper reaches of Hotan river were used to determine coefficient c and water depth index f. Finally, the average water depth index f was 0.36, and the value of coefficient c was 1.07. The value of river roughness coefficient n is provided by experts of hydrology bureau, and the value is 0.035. Combined with the field measurement of the river section of the edge slope, the obtained data as input data. On this basis, the river discharge of each river section was estimated through Equation (6), as shown in Table 4. Among them, the river width in 2017 were extracted from the UAV images.

Table 4. Estimated river discharge based on historical images.

	River-Course Cross-Sections	Hydraulic Slope (%)	Q (m^3/s)
P1	1993	2.31	1.15
	1997	2.31	10.86
	2010	2.31	14.40
	2017	2.31	2.306
P2	1993	1.32	0.67
	1997	1.32	6.05
	2010	1.32	8.71
	2017	1.32	1.317

In order to further analyze the water consumption situation after 100 km in the area of the desert reaches of the Hotan River for which there are no data, the river discharge of monitoring points P1 and P2 were counted from 1993 to 2017, and the results are shown in Table 5.

Table 5. Attenuation in the desert reaches of the Hotan River.

River-Course Cross-Sections	Attenuation (m^3/s)	Attenuation Coefficient (%)
1993	0.51	44.34
1997	4.55	41.74
2010	5.69	39.51
2017	0.989	42.89

According to the comparative analyses shown in Table 4, a loss of 0.48 m^3/s occurred within 100 km of the desert reaches of the Hotan River in 1993, and the loss percentage was 41.74%. In 1997, a loss of 4.81 m^3/s occurred within 100 km of the desert reaches of the Hotan River, and the loss percentage was 44.29%. In 2010, 5.69 m^3/s was lost within 100 km of the desert reaches of the Hotan River, and the loss percentage was 39.51%. In 2017, 0.989 m^3/s was lost within 100 km of the desert reaches of the Hotan River; the loss percentage was 42.89%. In general, the attenuation rate of the desert reaches of the Hotan River was <45%, and the attenuation coefficient tended to be consistent at approximately 40%.

6. Discussion

6.1. Parametric Sensitivity Analysis

According to Equation (6), the river discharge of hydrologic section in Kaqun were estimated. Coefficients a, c and f were key parameters in the flow estimation process. The relation between coefficient c and depth index f were obtained by calibration of the measured data of the hydrological station. Therefore, we only discussed the influence of coefficient a on the estimation results. Sichangi [73] research shows that for the trapezoidal section, coefficient a is shown in Equation (9). When river width >> depth, coefficient a can be approximately equal to $S^{1/2}/n$, as shown in Equation (10).

$$a_1 = \frac{S^{\frac{1}{2}}}{n(W + 2D\frac{1-\cos\theta}{\sin\theta})^{\frac{2}{3}}} \tag{9}$$

$$a_2 = \frac{S^{\frac{1}{2}}}{n} \tag{10}$$

where, S is hydraulic slope, n is roughness coefficient, W is water surface width, θ is edge slope, and D is average water depth. The width and depth of the channel were obtained every 0.5 m so as to establish the width-depth relationship of the channel. Finally, the coefficient D of this study was obtained by measuring the width of the river. The section of Kaqun hydrographic station was used as the experimental area to conduct a comparative study on the influence of the above two calculation methods of coefficient a on the estimation results, and the results were verified with the monthly average discharge data. The results were shown in Figure 10. On this basis, error analysis was conducted on the value results of different coefficients a, and the results were shown in Table 6.

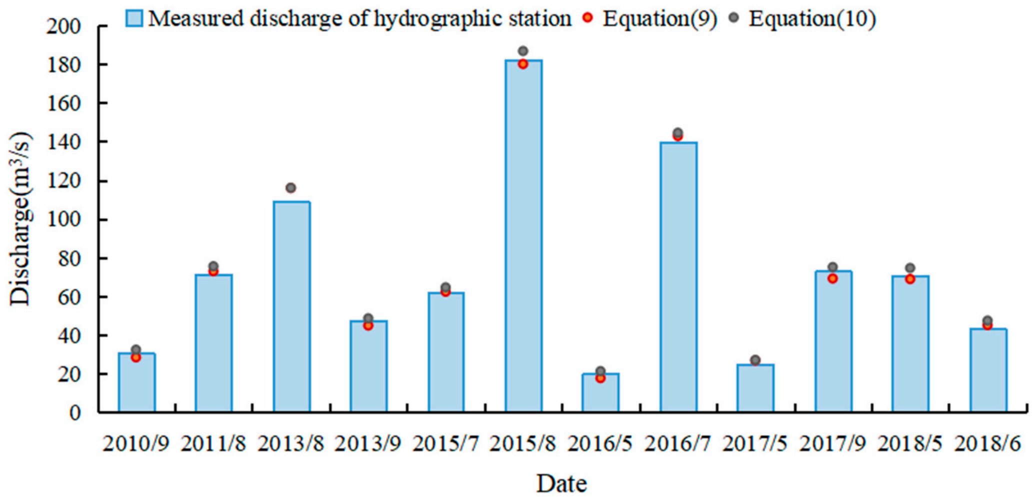

Figure 10. Flow estimation results under different coefficients a.

Table 6. Error analysis under different values of coefficient a.

River-Course Cross-Sections	RMSE (±m^3/s)	NSE (±)
Equation (9)	2.91	0.00
Equation (10)	12.77	0.01

The results showed that the coefficient a was approximately $S^{1/2}/n$ in Equation (10) for the section of Kaqun hydrologic station, and the estimated flow error were large. It is better to estimate the precision measured section of hydraulic slope obtained by combining low-altitude UAV with measured edge slope. Therefore, it is necessary to determine the calculation method of coefficient a according to the width-depth ratio of the river. When river width >> water depth, Equation (10) can be used to calculate a, while Equation (9) should be used for general wide and shallow rivers.

6.2. Uncertainty Evaluation

The river width of P1 and P2 sections of Hotan river in 1993, 1999 and 2010 were extracted by remote sensing images and compared with the river section width extracted by UAV images for verification. Errors caused by river width extracted from remote sensing images are evaluated by using RMSE. The uncertain results of discharge estimates associated with river width were shown in Table 7.

Table 7. Error in discharge estimation caused by measurements in river width (W) at gauging stations.

River-Course Cross-Sections	RMSE (±m^3/s)	
	P1	P2
1993	7.38	8.54
1999	6.89	7.96
2010	5.36	7.33

According to the river discharge estimation results of P1 and P2 sections of Hotan river in Section 5.2, the flow in dry season 2010 > 1999 > 1993. Combined with the error evaluation results, the measurement error of width in the years with low river discharge was larger, that was, the estimation error in 1993 was larger than that in other years. Moreover, the estimation error of upstream P1 section was smaller than that of downstream P2 section, which further indicated that with the decrease of river discharge, the error of width extraction increases, affecting the estimation accuracy.

6.3. The Attenuation Coefficients Are Compared with the Theoretical Results During the Dry Season

Generally, dry water flow is the type of runoff that can exist year-round in the course of a river, and it is the minimum water flow that can be maintained during the dry season [74]. In this study, the wetted perimeter method in hydraulics was used to further analyze and calculate the attenuation coefficients of Hotan River surface runoff, which has commonly been used in the estimation of dry water flow [75]. The wetted perimeter method is generally applicable to wide, shallow channels and paraboloid channels. Therefore, it is suitable for wide shallow river in the desert reaches of the Hotan River. It is relevant to note that Leopold and Maddock's analysis of the at-a-station hydraulic geometry found that the general relationship between channel width (closely related to the wetted perimeter) and discharge was a power function in the form of Equation (11) [62]:

$$P_w = Q^b \tag{11}$$

where P_w is the wetted perimeter in meters and Q is the river discharge (m^3/s). In general, the inflection point of the wetted perimeter change curve is found in the curve of wetted perimeter and river discharge. The river discharge value of this inflection point is regarded as the critical flow value of the flow in the river channel during the dry season [76].

In this study, sample points were selected at intervals of 0.5 m between the monitoring sections P1 and P2 in the desert reaches of the Hotan River using high-resolution images obtained from 1 December 2017 to 2 December 2017, where P1 included 50 sample points and P2 included 48 sample points. The river discharge and wetted perimeter of sample points P1 and P2 in the same period were calculated. Finally, the relationship between surface runoff and the wetted perimeter were calculated according to Equation (11). The results are shown in Figure 11.

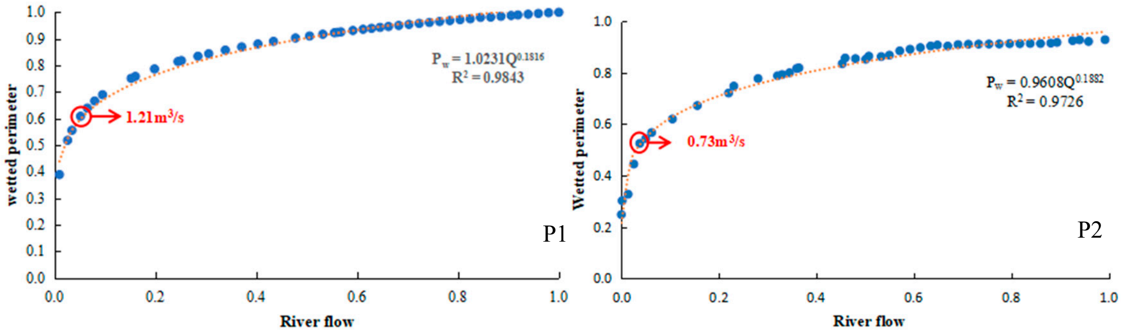

Figure 11. Relationships between the wetted perimeter and river discharge.

The results showed that the critical flow rate of sections P1 and P2 in the same period of dry water were 1.21 m^3/s and 0.73 m^3/s, respectively. On this basis, a critical flow difference of 0.48 m^3/s between sections P1 and P2 was calculated. At this point, the critical flow between the two sections decreases to 39.67%, and the results also tended to be 40%. The surface runoff satisfies the critical flow, and the attenuation coefficients of Hotan River natural channel is about 40%.

At the same time, these results were generally consistent with the calculated results of Huang [77]. They used 3 hydrological stations, 2 drainage channels, and connected the two tributaries as nodes to divide the river into 5 sub-sections, and then used a water-balance model to simulate Hotan River runoff. The results showed that the loss of surface runoff in the desert reaches of the Hotan River was 45.44%. These results were further supports the reliability of the calculated results of the attenuation coefficients in this study.

7. Conclusions

As an important source of water in the arid inland areas of northwest China, rivers play an important role in maintaining the integrity of river ecosystems. This study coupled UAV high-resolution images and remote sensing images, combined with the ground-based experimental data, to analyze the lowest attenuation coefficients of the Hotan River within 100 km in the case of an extreme drought season. The results revealed that:

1. Through Equation (6), the combination of low-altitude UAV remote sensing and high-altitude remote sensing can well realize the estimation of medium and small wide shallow rivers flow in arid areas.
2. Combined with satellite remote sensing images, the river discharge of the lower reaches of the Hotan River from 1993 to 2017 was estimated. Attenuation losses of surface runoff during this time were 0.51 m^3/s, 4.55 m^3/s, 5.69 m^3/s, and 0.99 m^3/s, respectively.
3. By calculating the attenuation coefficients from 1993 to 2017, the results showed that the attenuation coefficients of each year were 44.34%, 41.74%, 39.51%, and 42.89%, respectively. Therefore, the attenuation coefficients of the Hotan River appears to be stable at 40%.

Overall, the usage of UAVs to acquire channel parameters in this study provided a novel prospect for rapid river discharge assessments. With low-altitude UAV technologies, changes in the water conditions of monitoring sections and the lack of stations can be obtained according to the inversion flow results of a multi-phase UAV. Based on low-altitude remote sensing and satellite remote sensing, the attenuation coefficients of the Hotan River was deduced, and this provided abundant hydrological data for the desert in which there are few stations. Furthermore, the methods employed in this study can effectively promote research progress into basin river discharge and provide an important reference for global river discharge monitoring.

Author Contributions: Conceptualization, S.Y., J.W., P.W. and H.L.; Methodology, J.W.; Software, J.W., P.W. and H.L.; Project administration, T.G.; Visualization, J.W., P.W.; Writing—original draft preparation, J.W., P.W.

Funding: This research was funded by the National Natural Science Foundation of China (Grant Nos. U160320058).

Acknowledgments: We acknowledge all of the editors and reviewers for their valuable advice. The authors are also thankful for the financial support from the National Natural Science Foundation of China (Grant Nos. U160320058).

Conflicts of Interest: The authors declare no conflict of interest. The founding sponsors had no role in the design of the study; in the collection, analyses, or interpretation of data; in the writing of the manuscript; and in the decision to publish the results.

References

1. Shafroth, P.B.; Stromberg, J.C.; Pattern, D.T. Riparian vegetation response to altered disturbance and stress regimes. *Ecol. Appl.* **2002**, *12*, 107–123. [CrossRef]
2. Fekete, B.M.; Vörösmarty, C.J. The Current Status of Global River Discharge Monitoring and Potential New Technologies Complementing Traditional Discharge Measurements. In Proceedings of the PUB Kick-Off Meeting, Brasilia, Brazil, 20–22 November 2002; pp. 129–136.
3. Hao, X.; Li, W.; Huang, X.; Zhu, C.; Ma, J. Assessment of the groundwater threshold of desert riparian forest vegetation along the middle and lower reaches of the Tarim River, China. *Hydrol. Process.* **2010**, *24*, 178–186. [CrossRef]
4. Yang, X.; Liu, Z.; Zhang, F.; White, P.D.; Wang, X. Hydrological changes and land degradation in the southern and eastern Tarim Basin, Xinjiang, China. *Land Degrad. Dev.* **2006**, *17*, 381–392. [CrossRef]
5. Bullard, J.E.; McTainsh, G.H. Aeolian-fluvial interactions in dryland environments: Examples, concepts and Australia case study. *Pro. Phys. Geog.* **2003**, *27*, 471–501. [CrossRef]
6. Muhs, D.R.; Reynolds, R.L.; Been, J.; Skipp, G. Eolian sand transport pathways in the southwestern United States: Importance of the Colorado River and local sources. *Quat. Int.* **2003**, *104*, 3–18. [CrossRef]
7. Cole, K.L. Reconstruction of past desert vegetation along the Colorado River. *Palaeogeogr. Palaeocl.* **1990**, *76*, 349–366. [CrossRef]
8. Jin, H.L.; Dong, G.R. Preliminary Study on the Role of River Wriggling in the Evolution of Aeolian Landforms in Arid Region-Taking Hotan River as an Example. *J. Desert Res.* **2001**, *21*, 367–373. (In Chinese)
9. Rolls, R.J.; Leigh, C.; Sheldon, F. Mechanistic effects of low-flow hydrology on riverine ecosystems: Ecological principles and consequences of alteration. *Freshw. Sci.* **2012**, *31*, 1163–1186. [CrossRef]
10. Acuña, V.; Von Schiller, D.; García-Galán, M.J.; Rodríguez-Mozaz, S.; Corominas, L.; Petrovic, M.; Poch, M.; Barceló, D.; Sabater, S. Occurrence and in-stream attenuation of wastewater-derived pharmaceuticals in Iberian rivers. *Sci. Total Environ.* **2015**, *503*, 133–141. [CrossRef]
11. Gurr, C.J.; Reinhard, M. *Harnessing Natural Attenuation of Pharmaceuticals and Hormones in Rivers*; ACS: Washington, DC, USA, 2006.
12. Kunkel, U.; Radke, M. Biodegradation of acidic pharmaceuticals in bed sediments: Insight from a laboratory experiment. *Environ. Sci. Technol.* **2008**, *42*, 7273–7279. [CrossRef]
13. Tharme, R.E. A global perspective on environmental flow assessment: Emerging trends in the development and application of environmental flow methodologies for river. *River Res. Appl.* **2003**, *19*, 397–441. [CrossRef]
14. Soil and Water Assessment Tool: Theoretical Documentation Version 2005. Available online: https://oaktrust.library.tamu.edu/bitstream/handle/1969.1/128050/TR-406_Soil%20and%20Water%20Assessment%20Tool%20Theoretical%20Documentation.pdf?sequence=1 (accessed on 12 December 2019).
15. McIntyre, N.; Al-Qurashi, A. Performance of ten rainfall–runoff models applied to an arid catchment in Oman. *Environ. Model. Softw.* **2009**, *24*, 726–738. [CrossRef]
16. Radchenko, I.; Dernedde, Y.; Mannig, B.; Frede, H.G.; Breuer, L. Climate change impacts on runoff in the Ferghana Valley (Central Asia). *Water Resour.* **2017**, *44*, 707–730. [CrossRef]
17. Blöschl, G.; Sivapalan, M.; Savenije, H.; Wagener, T.; Viglione, A. *Runoff Prediction in Ungauged Basins: Synthesis Across Processes, Places and Scales*; Cambridge University Press: Cambridge, UK, 2013.
18. Sivapalan, M.; Takeuchi, K.; Franks, S.W.; Gupta, V.K.; Karambiri, H.; Lakshmi, V.; Liang, X.; Mcdonnell, J.; Mendiondo, M.E.; Connell, O.; et al. IAHS Decade on Predictions in Ungauged Basins (PUB), 2003–2012: Shaping an exciting future for the hydrological sciences. *Hydrol. Sci. J.* **2003**, *48*, 857–880. [CrossRef]
19. Young, A.R. Stream flow simulation within UK ungauged catchments using a daily rainfall-runoff model. *J. Hydrol.* **2006**, *320*, 155–172. [CrossRef]
20. Mishra, A.K.; Coulibaly, P. Developments in hydrometric network design: A review. *Rev. Geophys.* **2009**, *47*. [CrossRef]
21. Lacroix, K.E.M.; Tapia, E.; Springer, A. Environmental flows in the desert rivers of the United States and Mexico: Synthesis of available data and gap analysis. *J. Arid. Environ.* **2017**, *140*, 67–78. [CrossRef]
22. Liu, S.; Xie, Z.; Zeng, Y. Discharge estimation for an ungauged inland river in an arid area related to anthropogenic activities: A case study of Heihe River Basin, Northwestern China. *Adv. Meteorol.* **2016**, *2016*, 1–11. [CrossRef]

23. Seibert, J.; Beven, K.J. Gauging the ungauged basin: How many discharge measurements are needed? *Hydrol. Earth Syst. Sci.* **2009**, *13*, 883–892. [CrossRef]
24. Writer, J.H.; Keefe, S.K.; Ryan, J.N.; Ferrer, I.; Thurman, M.E.; Barber, L.B. Methods for evaluating in-stream attenuation of trace organic compounds. *Appl. Geochem.* **2011**, *26*, S344–S345. [CrossRef]
25. Fenner, K.; Canonica, S.; Wackett, L.P.; Elsner, M. Evaluating pesticide degradation in the environment: Blind spots and emerging opportunities. *Science* **2013**, *341*, 752–758. [CrossRef] [PubMed]
26. Sun, W.C.; Ishidaira, H.; Bastola, S. Towards improving river discharge estimation in ungauged basins: Calibration of rainfall-runoff models based on satellite observations of river discharge width at basin outlet. *Hydrol. Earth Syst. Sci.* **2010**, *14*, 2011–2022. [CrossRef]
27. Nathanson, M.; Kean, J.W.; Grabs, T.J.; Seibert, J.; Laudon, H.; Lyon, S.W. Modelling rating curves using remotely sensed LiDAR data. *Hydrol. Process.* **2012**, *26*, 1427–1434. [CrossRef]
28. Khromova, T.E.; Osipova, G.B.; Tsvetkov, D.G.; Dyurgerov, M.B.; Barry, R.G. Changes in glacier extent in the eastern Pamir, Central Asia, determined from historical data and ASTER imagery. *Remote Sens. Environ.* **2006**, *102*, 24–32. [CrossRef]
29. Merz, R.; Blöschl, G. Regionalisation of catchment model parameters. *J. Hydrol.* **2004**, *287*, 95–123. [CrossRef]
30. Jin, X.; Xu, C.Y.; Zhang, Q.; Chen, Y.D. Regionalization study of a conceptual hydrological model in Dongjiang basin, south China. *Quat. Int.* **2009**, *208*, 129–137. [CrossRef]
31. Schulze, K.; Hunger, M.; Döll, P. Simulating river discharge velocity on global scale. *Adv. Geosci.* **2005**, *5*, 133–136. (In Chinese) [CrossRef]
32. O'Hare, M.T.; McGahey, C.; Bissett, N.; Cailes, C.; Henville, P.; Scarlett, P. Variability in roughness measurements for vegetated rivers near base flow, in England and Scotland. *J. Hydrol.* **2010**, *385*, 361–370. [CrossRef]
33. Dibike, Y.B.; Solomatine, D.P. River flow forecasting using artificial neural networks. *Phys. Chem. Earth Part B Hydrol. Ocean. Atmos.* **2001**, *26*, 1–7. [CrossRef]
34. Solomatine, D.P.; Shrestha, D.L. A novel method to estimate model uncertainty using machine learning techniques. *Water Resour. Res.* **2009**, *45*. [CrossRef]
35. Widén-Nilsson, E.; Halldin, S.; Xu, C.Y. Global water-balance modelling with WASMOD-M: Parameter estimation and regionalisation. *J. Hydrol.* **2007**, *340*, 105–118. [CrossRef]
36. Hannah, D.M.; Demuth, S.; van Lanen, H.A.; Looser, U.; Prudhomme, C.; Rees, G.; Stahl, K.; Tallaksen, L.M. Large-scale river flow archives: Importance, current status and future needs. *Hydrol. Process.* **2011**, *25*, 1191–1200. [CrossRef]
37. Pavelsky, T.M. Using width-based rating curves from spatially discontinuous satellite imagery to monitor river discharge. *Hydrol. Process.* **2014**, *28*, 3035–3040. [CrossRef]
38. Tarpanelli, A.; Brocca, L.; Lacava, T.; Melone, F.; Moramarco, T.; Faruolo, M.; Pergola, N.; Tramutoli, V. Toward the estimation of river discharge variations using MODIS data in ungauged basins. *Remote Sens. Environ.* **2013**, *136*, 47–55. [CrossRef]
39. Colomina, I.; Molina, P. Unmanned aerial systems for photogrammetry and remote sensing: A review. *ISPRS J. Photogramm. Remote Sens.* **2014**, *92*, 79–97. [CrossRef]
40. Bertalan, L.; Novák, T.; Németh, Z.; Rodrigo-Comino, J.; Kertész, Á.; Szabó, S. Issues of Meander Development: Land Degradation or Ecological Value? The Example of the Sajó River, Hungary. *Water* **2018**, *10*, 1613. [CrossRef]
41. Rusnák, M.; Sládek, J.; Kidová, A.; Lehotský, M. Template for high-resolution river landscape mapping using UAV technology. *Measurement* **2018**, *115*, 139–151. [CrossRef]
42. Singh, K.K.; Frazier, A.E. A meta-analysis and review of unmanned aircraft system (UAS) imagery for terrestrial applications. *Int. J. Remote Sens.* **2018**, *39*, 5078–5098. [CrossRef]
43. Manfreda, S.; McCabe, M.F.; Miller, P.E.; Lucas, R.; Pajuelo Madrigal, V.; Mallinis, G.; Ben Dor, E.; Helman, D.; Estes, L.; Ciraolo, G.; et al. On the use of unmanned aerial systems for environmental monitoring. *Remote Sens.* **2018**, *10*, 641. [CrossRef]
44. Zhao, C.S.; Zhang, C.B.; Yang, S.T.; Liu, C.M.; Xiang, H.; Sun, Y.; Yang, Z.Y.; Zhang, Y.; Yu, X.Y.; Shao, N.F.; et al. Calculating e-flow using UAV and ground monitoring. *J. Hydrol.* **2017**, *552*, 351–365. [CrossRef]
45. Hemmelder, S.; Marra, W.; Markies, H.; De Jong, S.M. Monitoring river morphology & bank erosion using UAV imagery—A case study of the river Buëch, Hautes-Alpes, France. *Int. J. Appl. Earth Obs. Geoinf.* **2018**, *73*, 428–437.

46. Casado, M.; Gonzalez, R.; Kriechbaumer, T.; Veal, A. Automated identification of river hydromorphological features using UAV high resolution aerial imagery. *Sensors* **2015**, *15*, 27969–27989. [CrossRef] [PubMed]
47. Yang, S.; Wang, P.; Lou, H.; Wang, J.; Zhao, C.; Gong, T. Estimating River Discharges in Ungauged Catchments Using the Slope—Area Method and Unmanned Aerial Vehicle. *Water* **2019**, *11*, 2361. [CrossRef]
48. Vivoni, E.R.; Rango, A.; Anderson, C.A.; Pierini, N.A.; Schreiner-McGraw, A.P.; Saripalli, S.; Laliberte, A.S. Ecohydrology with unmanned aerial vehicles. *Ecosphere* **2014**, *5*, 1–14. [CrossRef]
49. Jordan, B.R. A bird's-eye view of geology: The use of micro drones/UAVs in geologic fieldwork and education. *GSA Today* **2015**, *25*, 50–52. [CrossRef]
50. Clapuyt, F.; Vanacker, V.; Van, O.K. Reproducibility of UAV-based earth topography reconstructions based on Structure-from-Motion algorithms. *Geomorphology* **2016**, *260*, 4–15. [CrossRef]
51. Hagg, W.; Braun, L.N.; Kuhn, M.; Nesgaard, T.I. Modelling of hydrological response to climate change in glacierized Central Asian catchments. *J. Hydrol.* **2007**, *332*, 40–53. [CrossRef]
52. Li, C.; Lei, J.; Zhao, Y.; Xu, X.; Li, S. Effect of saline water irrigation on soil development and plant growth in the Taklimakan Desert Highway shelterbelt. *Soil Till. Res.* **2015**, *146*, 99–107. [CrossRef]
53. Wang, K.; He, Q.; Wang, M.Z.; Hu, Y.H.; Li, X.H. Wind field at boundary layer in hinterland of the Taklimakan Desert. *J. Desert Res.* **2012**, *29*, 302–305.
54. Zhang, J.; Takahashi, K.; Wushiki, H.; Yabuki, S.; Xiong, J.M.; Masuda, A. Water geochemistry of the rivers around the Taklimakan Desert (NW China): Crustal weathering and evaporation processes in arid land. *Chem. Geol.* **1995**, *119*, 225–237. [CrossRef]
55. Yan, P.; Li, X.; Ma, Y.; Wu, W.; Qian, Y. Morphological characteristics of interactions between deserts and rivers in northern China. *Aeolian Res.* **2015**, *19*, 225–233. [CrossRef]
56. Yu, Y.; Huang, L.M.; Sheng, B.; Maimaitiming, A.; Qing, S.Y.; Dai, Y.P. Current situation analysis of water consumption in hotan river basin. *J. Water Resour. Water Eng.* **2009**, *20*, 47–51. (In Chinese)
57. Powell, R.W. The origin of Manning's formula. *J. Hydraul. Div.* **1968**, *94*, 1179–1181.
58. De Doncker, L.; Troch, P.; Verhoeven, R.; Bal, K.; Meire, P.; Quintelier, J. Determination of the Manning roughness coefficient influenced by vegetation in the river Aa and Biebrza river. *Environ. Fluid Mech.* **2009**, *9*, 549–567. [CrossRef]
59. Noarayanan, L.; Murali, K.; Sundar, V. Manning's "n" co-efficient for flexible emergent vegetation in tandem configuration. *J. Hydro Environ. Res.* **2012**, *6*, 51–62. [CrossRef]
60. Ngo-Duc, T.; Oki, T.; Kanae, S. Avariable streamflow velocity method for global river routing model: Model description and preliminary results. *Hydrol. Earth Syst. Sci.* **2007**, *4*, 4389–4414. [CrossRef]
61. Huang, Q.; Long, D.; Du, M.; Zeng, C.; Qiao, G.; Li, X.; Hou, A.; Hong, Y. Discharge estimation in high-mountain regions with improved methods using multisource remote sensing: A case study of the Upper Brahmaputra River. *Remote Sens. Environ.* **2018**, *219*, 115–134. [CrossRef]
62. Leopold, L.B.; Maddock, T. The hydraulic geometry of stream channels and some physiographic implications. *Geol. Surv. Prof. Pap.* **1953**, *252*, 57.
63. Neitzel, F.; Klonowski, J. Mobile 3D mapping with a low-cost UAV system. *Int. Arch. Photogramm. Remote Sens. Spat. Inf. Sci.* **2011**, *38*, 1–6. [CrossRef]
64. Harder, P.; Schirmer, M.; Pomeroy, J.; Helgason, W. Accuracy of snow depth estimation in mountain and prairie environments by an unmanned aerial vehicle. *Cryosphere* **2016**, *10*, 2559. [CrossRef]
65. Neugirg, F.; Stark, M.; Kaiser, A.; Vlacilova, M.; Della Seta, M.; Vergari, F.; Schmidt, J.; Becht, M.; Haas, F. Erosion processes in calanchi in the Upper Orcia Valley, Southern Tuscany, Italy based on multitemporal high-resolution terrestrial LiDAR and UAV surveys. *Geomorphology* **2016**, *269*, 8–22. [CrossRef]
66. Ruzgienė, B.; Berteška, T.; Gečyte, S.; Jakubauskienė, E.; Aksamitauskas, V.Č. The surface modelling based on UAV Photogrammetry and qualitative estimation. *Measurement* **2015**, *73*, 619–627. [CrossRef]
67. Turner, D.; Lucieer, A.; Wallace, L. Direct georeferencing of ultrahigh-resolution UAV imagery. *IEEE Trans. Geosci. Remote* **2014**, *52*, 2738–2745. [CrossRef]
68. Nash, J.E.; Sutcliffe, J.V. River discharge forecasting through conceptual models part I—A discussion of principles. *J. Hydrol.* **1970**, *10*, 282–290. [CrossRef]
69. Xu, H. A study on information extraction of water body with the modified normalized difference water index (MNDWI). *J. Remote Sens.* **2005**, *9*, 589–595.
70. Otsu, N. A threshold selection method from gray-level histograms. *IEEE Trans. Syst. Man Cybern.* **1979**, *9*, 62–66. [CrossRef]

71. Chanson, H. *Environmental Hydraulics for Open Channel Flows*; Elsevier: Amsterdam, The Netherlands, 2004.
72. Wang, J.; Wang, J.; Sun, X. Analysis of water change along Hotan river basin. *J. Water Resour. Water Eng.* **2013**, *24*, 142–148. (In Chinese)
73. Sichangi, A.W.; Wang, L.; Yang, K.; Chen, D.; Wang, Z.; Li, X.; Zhou, J.; Liu, W.; Kuria, D. Estimating continental river basin discharges using multiple remote sensing data sets. *Remote Sens. Environ.* **2016**, *179*, 36–53. [CrossRef]
74. Wu, X.; Li, H.; Dong, Y.; Lin, Q. Calculation of ecological basic flow of Weihe River based on basic flow ratio method. *Trans. Chin. Soc. Agric. Eng.* **2011**, *27*, 154–159. (In Chinese)
75. Hughes, D.A.; Hannart, P. A desktop model used to provide an initial estimate of the ecological in-stream flow requirements of rivers in South Africa. *J. Hydrol.* **2003**, *270*, 167–181. [CrossRef]
76. Gippel, C.J.; Stewardson, M.J. Use of wetted perimeter in defining minimum environmental flows. *Regul. Rivers Res. Manag.* **1998**, *14*, 53–67. [CrossRef]
77. Huang, L.M.; Sheng, B.; Wang, Z.R.; Qing, S.Y.; Yin, R.H. Surface runoff simulation of Hetian river in Xinjiang. *Acta Univ. Agric. Boreali-Occidentalis.* **2000**, *3*, 45–50. (In Chinese)

© 2019 by the authors. Licensee MDPI, Basel, Switzerland. This article is an open access article distributed under the terms and conditions of the Creative Commons Attribution (CC BY) license (http://creativecommons.org/licenses/by/4.0/).